3D Tensor Reconstruction in X-ray Dark-field Tomography – The First Phantom Result

Shiyang Hu[1,2], Christian Riess[1,3], Joachim Hornegger [1,2], Peter Fischer [1,2], Florian Bayer [4], Thomas Weber[4], Gisela Anton[4], Andreas Maier[1]

[1]Pattern Recognition Lab, Department of Computer Science, Friedrich-Alexander University of Erlangen-Nuremberg, Erlangen, Germany
[2]Erlangen Graduate School in Advanced Optical Technologies (SAOT), Friedrich-Alexander University of Erlangen-Nuremberg, Erlangen, Germany
[3]Department of Radiology, Stanford University, Stanford, California
[4]Erlangen Centre for Astroparticle Physics (ECAP), Friedrich-Alexander University of Erlangen-Nuremberg, Erlangen, Germany
shiyang.hu@fau.de

Abstract. X-ray dark-field imaging is a novel technique which provides complementary information on structural variation and density fluctuation. It allows to obtain object structures at micrometer scale and also contains information on the orientation of these structures. Since it can be acquired by a conventional X-ray imaging system, dark-field imaging has great potential for medical diagnosis.
However, fully recovering 3D orientations in dark-field reconstruction still remains unexplored. In this paper, we propose an improved reconstruction method based on the zero-constrained dark-field reconstruction by Bayer *et al.* and a simplified principle axes transformation. A well-defined phantom containing representative 3D orientations is reconstructed in our experiment. On average, the structure orientations in the reconstructed volume differ from the ground truth by 9%. Within the boundaries of an object, the error drops to 6%. Application of this method in real diagnosis data can be expected in future.

1 Introduction

X-ray dark-field imaging reveals ultra-small-angle scattering. It has attracted attention in recent years for providing unprecedented information [1]. Such images are usually obtained by Talbot-Lau grating interferometer with conventional X-ray tube and detectors [2,3]. Ultra-small-angle scattering is generated by local orientations of microstructures in the order of magnitude of the grating period. Thus dark-field imaging allows reconstruction of structures at length scales below the resolution of conventional X-ray imaging systems. Dark-field reconstruction shows great potential for medical diagnosis and specimens in nondestructive materials testing. One promising application is the diagnosis of osteoporosis where detection of different bone structures is required. Micrometer-sized calcifications in mammography have been observed in dark-field imaging by Michel *et al.* [4],

which is currently investigated for its suitability for early detection of breast cancer.

Previous work presented experiments in dark-field radiography and observations of periodical dark-field signals caused by structural variation. Several groups partially reconstructed local orientations. Revol *et al.* exploited prior knowledge on microstructure orientations to separate isotropic and anisotropic components [5]. Malecki *et al.* formulated contributions of scattering and sensitivity for each voxel [6]. However, a full 3D reconstruction of vectorial information of the imaging object with separated isotropic and anisotropic contributions is still not available. Bayer *et al.* [7] successfully reconstructed scalar and vectorial components in dark-field tomography and presented several test specimens. However, the reconstructed local orientation is the projected angle from 3D local orientation and it remains in a 2D plane. In this paper, we present an approach to extend the tensorial information to 3D. This improved method reconstructs two sets of projection data from different imaging coordinate systems and registers them into the same object to acquire fully three-dimensional structures. The proposed method demonstrates that two tomographic scans in different trajectories suffice to recover the microstructure orientation with great accuracy.

2 Materials and Methods

The proposed algorithm works as follows:

1. Reconstruct two sets of dark-field signal by gradient descent method with zero constraints.
2. Register reconstructed results from Step 1 into the same system by center of mass alignment.
3. Calculate 3D local orientation by in-plane angle from Step 1 according to Equation 2.

2.1 Two Imaging Models

Two sets of dark-field projections in different imaging coordinate systems are required for the proposed method. As illustrated in Fig. 1, the object in projection model A is located in the position such that its $\hat{y}$-axis is along y-axis in world coordinate system and is scanned around $\hat{y}$-axis. In projection model B, the $\hat{x}$-axis of the object coordinate system, around which the object is scanned, is aligned with y-axis in world coordinate system.

We reconstruct each set of projections using the gradient descent method with zero constraints proposed in Bayer *et al.* [7]. This computation provides for both image planes the in-plane local orientation as well as its isotropic and anisotropic contributions.

The phantom dimensions are denoted as $M \times N \times L$, $\theta^y, d^y_{iso}, d^y_{aniso}$ denote reconstructed orientations in the $X - Z$ plane and their isotropic and anisotropic contributions to dark-field signal from projection model A, respectively. $d^x_{iso}, d^x_{aniso}, \theta^x$ represent reconstructed isotropic components, anisotropic

components and local orientations in $Y-Z$ plane from projection Model B, respectively.

2.2 Registration

Before calculating 3D structures from reconstructed results described above, it is necessary to register both results into the same object due to mechanical instability in the experiments. Therefore, we introduce a simplified principal axes transformation here [8]. In this registration step, we register two sets of data by aligning their center of mass, which is calculated by position (x, y, z) and the isotropic component $d_{iso}(x, y, z)$ at that position. $d_{iso}(x, y, z) = d^{y}_{iso}(x, y, z)$ in projection model A and $d_{iso}(x, y, z) = d^{x}_{iso}(x, y, z)$ in projection model B. The center of mass can be expressed as:

$$C(d) = [x_c, y_c, z_c] := \frac{\sum_{i=1}^{M}\sum_{j=1}^{N}\sum_{k=1}^{L} d_{iso}(x_i, y_j, z_k) \cdot (x_i, y_j, z_k)}{\sum_{i=1}^{M}\sum_{j=1}^{N}\sum_{k=1}^{L} d_{iso}(x_i, y_j, z_k)} \tag{1}$$

Between the two projection models, we only move the object rigidly. Since we already know the axis around which the object rotates in the two models, only translation needs to be calculated. Thus the center of mass provides sufficient information for our registration. However, we expect that we will require a more sophisticated transform for real data, which is subject to future work.

2.3 3D Orientation Reconstruction

3D local orientations are calculated from two sets of reconstructed in-plane angles after the registration step. If the unknown orientation is parallel to $\hat{y}$-axis or $\hat{x}$-axis, it will only show isotropic scattering when rotating around the axis it is parallel to. To avoid infinite from tangent, the orientation is set as $(0, 1, 0)$ if $\theta_x = 90°$. A 3D orientation, which is denoted by a unit vector (v_x, v_y, v_z) can be obtained by:

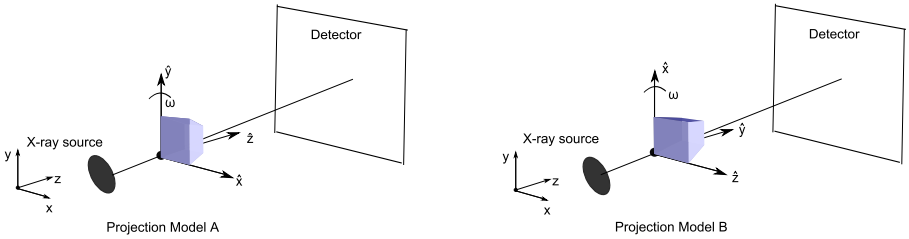

Fig. 1. Two imaging models with different object orientation.

$$[v_x, v_y, v_z] = \begin{cases} (1,0,0) & \text{if } d^x_{aniso} = 0 \\ (0,1,0) & \text{if } d^y_{aniso} = 0 \\ (0,1,0) & \text{if } \quad \theta_x = 90° \\ \frac{(\cos(\theta_y), \sin(\theta_y)\tan(\theta_x), \sin(\theta_y))}{\|(\cos(\theta_y), \sin(\theta_y)\tan(\theta_x), \sin(\theta_y))\|} & \text{otherwise} \end{cases} \tag{2}$$

2.4 Experiment

For the tomography scans, 101 projections were taken over 360° for both projection models. For reconstruction, 100 iterative steps have been taken for each projection model.

3 Results

The 3D local orientation dark-field tomography reconstruction was evaluated using a well-defined phantom (Fig. 2, Column A). This phantom was created as a mathematical block of $20 \times 25 \times 30$ pixels in an imaging space of $50 \times 50 \times 50$ pixels. To simulate two imaging models and their mechanical instability, the phantom was positioned differently in each projection model. In projection model A, the center of phantom was located at position $(26, 22, 21)$ in the world system. In projection model B, the center of phantom was positioned at $(28, 25, 16)$ in the world system. The phantom has the isotropic parameter $d_{iso}(\hat{x}, \hat{y}, \hat{z}) \equiv 1.0$ and anisotropic parameter $d_{aniso}(\hat{x}, \hat{y}, \hat{z}) \equiv 1.5$. Different local orientations are obtained in five sub-blocks among $\hat{y}$-axis. These orientations are visualized in Fig. 2, Column A1 and Column A2.

From calculation of registration step, center of mass in projection model A is $(26, 22, 21)$ and center of mass in projection model B is $(28, 25, 16)$. This result matches our phantom design.

Reconstructed results are visualized in Fig 2, Column B1 and Column B2. Five representative layers from each sub-block are visualized and compared with the same layer from ground truth in Column A1 and Column A2. Visualization was created using ParaView. The microstructure, which can be represented by $(d_{aniso}v_x, d_{aniso}v_y, d_{aniso}v_z)$ are visualized by lines. The length of each line is the magnitude of its anisotropic component. Orientations are visualized by the line directions. Five representative layers from five sub-blocks are shown in Fig 2 from top to bottom for both phantom and reconstructed results.

To quantitatively evaluate our algorithm, we calculated the error between reconstructed orientation and ground truth. Error per voxel at position (x, y, z) is defined as:

$$e_{pv} = \|(v^\star_x(x,y,z), v^\star_y(x,y,z), v^\star_z(x,y,z)) - (v_x(x,y,z), v_y(x,y,z), v_z(x,y,z))\| \tag{3}$$

where $(v^\star_x, v^\star_y, v^\star_z)$ is a unit vector which denotes local orientation in ground truth.

Fig 3 shows error per voxel from the five representative layers by color legend of magnitude. Empty space in this visualization implies zero error.

To measure the average error of reconstructed result, we introduce average reconstruction error as:

$$e_v = \frac{\sum_{x,y,z} \|(v_x^\star, v_y^\star, v_z^\star) - (v_x, v_y, v_z)\|}{N \cdot M \cdot L} \tag{4}$$

In our experiment, the average reconstruction error is 0.091. Fig 3 shows that most errors are caused by edges, this is also a limitation of the reconstruction method in Bayer *et al.* [7]. Thus we also calculated this average reconstruction error without edges, i.e phantom with dimensions $(N-4) \times (M-4) \times L$, this gives us a smaller error of 0.059.

4 Discussion

In this paper, a new approach to reconstruct 3D orientations is presented. The major improvement of this proposed method is to fully recover vectorial information in a scanned object. Two sets of projections from different imaging coordinate systems are required as inputs. Mechanical instability of the imaging systems is compensated by a registration step and thus no further prior knowledge is needed. A shift in center of mass is corrected in this registration step. Visualized microstructure of the well-defined phantom showed that this method is able to reconstruct 3D local orientations. Error measurement shows orientations from reconstructed results have error by 9% from orientations of the phantom and 6% if we omitted edges.

This algorithm shows great potential of dark-field imaging by its ability of providing unique information using a conventional X-ray imaging system. Real

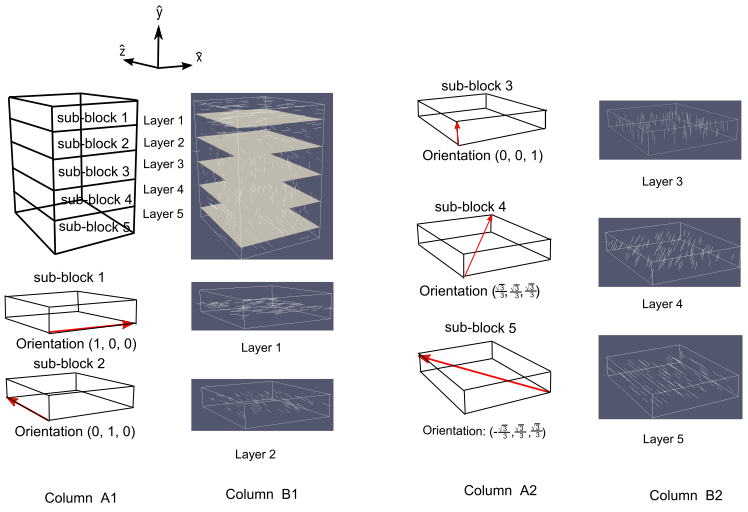

Fig. 2. Orientations from the phantom and reconstructed results. Five representative layers are visualized to show different orientations in each sub-block.

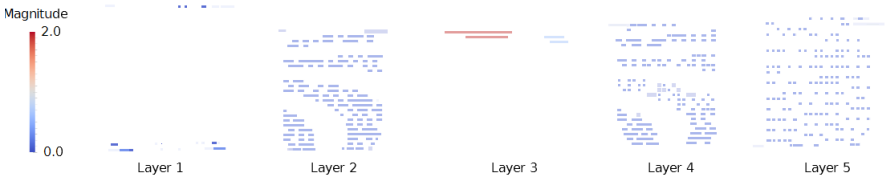

Fig. 3. Visualization of error per voxel at five representative layers according to equation 3. Empty space denotes zero.

data will be examined in our future work. Furthermore, we will investigate how much the axes must deviate to reconstruct a correct image.

5 Acknowledgment

The authors acknowledge funding of the Erlangen Graduate School in Advanced Optical Technologies (SAOT) by the German Research Foundation (DFG) in the framework of the German excellence initiative. Furthermore, we acknowledge support from the RTG 1773 by the German Research Foundation.

References

1. Kaeppler S, Bayer F, Weber T, Maier A, Anton G, Hornegger J, et al. Signal Decomposition for X-ray Dark-Field Imaging. Medical Image Computing and Computer-Assisted Intervention - MICCAI 2014. 2014;8673:170–177.
2. Pfeiffer F, Bech M, Bunk O, Kraft P, Eikenberry EF, Brönnimann C, et al. Hard-X-ray dark-field imaging using a grating interferometer. Nature materials. 2008;7(2):134–137.
3. Yashiro W, Terui Y, Kawabata K, Momose A. On the origin of visibility contrast in x-ray Talbot interferometry. Optics express. 2010;18(16):16890–16901.
4. Michel T, Rieger J, Anton G, Bayer F, Beckmann MW, Durst J, et al. On a dark-field signal generated by micrometer-sized calcifications in phase-contrast mammography. Physics in medicine and biology. 2013;58(8):2713.
5. Revol V, Kottler C, Kaufmann R, Neels A, Dommann A. Orientation-selective X-ray dark field imaging of ordered systems. Journal of Applied Physics. 2012;112(11):114903.
6. Malecki A, Potdevin G, Biernath T, Eggl E, Willer K, Lasser T, et al. X-ray tensor tomography. EPL (Europhysics Letters). 2014;105(3):38002.
7. Bayer FL, Hu S, Maier A, Weber T, Anton G, Michel T, et al. Reconstruction of scalar and vectorial components in X-ray dark-field tomography. Proceedings of the National Academy of Sciences. 2014;111(35):12699–12704.
8. Modersitzki J. Numerical methods for image registration. OUP Oxford; 2003.